

# THE TOPOLOGICAL SUSCEPTIBILITY AND $f_\pi$ FROM LATTICE QCD

*UKQCD Collaboration*

A. Hart<sup>a</sup> and M. Teper<sup>b</sup>

<sup>a</sup>*Department of Applied Mathematics and Theoretical Physics,  
Centre for Mathematical Sciences, University of Cambridge,  
Wilberforce Road CB3 0WA, UK*

<sup>b</sup>*Theoretical Physics, University of Oxford, 1 Keble Road,  
Oxford OX1 3NP, UK*

## **Abstract.**

We study the topological susceptibility,  $\chi$ , in QCD with two quark flavours using lattice field configurations that have been produced with an  $O(a)$  improved quark action. We find clear evidence for the expected suppression at small quark mass, and examine the variation of  $\chi$  with this mass. The resulting estimate of the pion decay constant,  $f_\pi = 105 \pm 6 \begin{smallmatrix} +18 \\ -10 \end{smallmatrix}$  MeV, is consistent with the experimental value of  $\simeq 93$  MeV. We compare  $\chi$  to the large- $N_c$  prediction and find consistency over a large range of quark masses. We discuss the benefits of the non-perturbative action improvement scheme and of the strategy of keeping the lattice spacing (nearly) fixed as the quark mass is varied. We compare our results with other studies and suggest why such a quark mass dependence has not always been seen.

# 1 Introduction

In gluodynamics (the pure gauge or “quenched” theory) lattice calculations of the continuum topological susceptibility now appear to be relatively free of the systematic errors arising from the discretisation, the finite volumes and the various measurement algorithms employed (for a recent review, see [1]).

The inclusion of sea quarks in (“dynamical”) lattice simulations, even at the relatively large quark masses currently employed, is numerically extremely expensive, and can only be done for lattices with relatively few sites (typically  $16^3 32$ ). To avoid significant finite volume errors, the lattice must then be relatively coarse, with, in our case, a spacing  $a \simeq 0.1$  fm. This is a significant fraction of the mean instanton radius, as calculated in gluodynamics, and thus precludes a robust, detailed study of the local topological features of the vacuum in the presence of sea quarks. The topological susceptibility, on the other hand, may be calculated with some confidence and provides one of the first opportunities to test some of the more interesting predictions of QCD. Indeed, it is in these measurements that we find some of the most striking evidence for the presence of the sea quarks (or, alternatively, for a strong quenching effect) in the lattice simulations.

We recall that the ensembles used here have been produced with two notable features [2]. The first is the use of an improved action, such that leading order lattice discretisation effects are expected to depend quadratically, rather than linearly, on the lattice spacing (just as in gluodynamics). In addition, the action parameters have been chosen to maintain a relatively constant lattice spacing, particularly for the larger values of the quark mass.

These features have allowed us to see the first clear evidence [3] for the expected suppression of the topological susceptibility in the chiral limit, despite our relatively large quark masses. From this behaviour we can directly estimate the pion decay constant without needing to know the lattice operator renormalisation factors that arise in more conventional calculations.

The structure of this paper is as follows. In Section 2 we discuss the measurement of the topological susceptibility and its expected behaviour both near the chiral limit, and in the limit of a large number of colours,  $N_c$ . In Section 3 we describe the UKQCD ensembles and the lattice measurements of the topological susceptibility over a range of sea quark masses. We fit these with various ansätze motivated by the previous section. We compare our findings with other recent studies in Section 4. Finally, we provide a summary in Section 5.

These results were presented at the IOP2000 [3], the Confinement IV [4] and, in a much more preliminary form, the Lattice '99 [5] conferences. Since then, we have increased the size of several ensembles and included a new parameter set to try and address the issue of discretisation effects in our results. We also have more accurate results from the quenched theory with which to compare. A brief summary of this work appears in [2].

## 2 The topological susceptibility

In four-dimensional Euclidean space-time, SU(3) gauge field configurations can be separated into topological classes, and moving between different classes is not possible by a smooth deformation of the fields. The classes are characterised by an integer-valued winding number. This Pontryagin index, or topological charge  $Q$ , can be obtained by integrating the local topological charge density

$$q(x) = \frac{1}{2} \varepsilon_{\mu\nu\sigma\tau} F_{\mu\nu}^a(x) F_{\sigma\tau}^a(x) \quad (1)$$

over all space-time

$$Q = \frac{1}{32\pi^2} \int q(x) d^4x. \quad (2)$$

The topological susceptibility is the expectation value of the squared charge, normalised by the volume

$$\chi = \frac{\langle Q^2 \rangle}{V}. \quad (3)$$

An isolated topological charge induces an exact zero-mode in the quark Dirac operator. As a result sea quarks in the vacuum induce an instanton–anti-instanton attraction which becomes stronger as the quark masses,  $m_u, m_d, \dots$ , decrease towards zero (the ‘chiral limit’), and the topological charge and susceptibility will be suppressed to leading order in the quark mass [6],

$$\chi = \Sigma \left( \frac{1}{m_u} + \frac{1}{m_d} \right)^{-1} \quad (4)$$

where

$$\Sigma = - \lim_{m_q \rightarrow 0} \lim_{V \rightarrow \infty} \langle 0 | \bar{\psi} \psi | 0 \rangle \quad (5)$$

is the chiral condensate (see [7] for a recent discussion). Here we have assumed  $\langle 0 | \bar{\psi} \psi | 0 \rangle = \langle 0 | \bar{u} u | 0 \rangle = \langle 0 | \bar{d} d | 0 \rangle$  and we neglect the contribution of heavier quarks. PCAC theory relates this to the pion decay constant  $f_\pi$  and mass  $M_\pi$  via the Gell-Mann–Oakes–Renner relation as

$$f_\pi^2 M_\pi^2 = (m_u + m_d) \Sigma + \mathcal{O}(m_q^2) \quad (6)$$

and we may combine these for  $N_f$  degenerate light flavours to obtain

$$\chi = \frac{f_\pi^2 M_\pi^2}{2N_f} + \mathcal{O}(M_\pi^4) \quad (7)$$

in a convention where the experimental value of  $f_\pi \simeq 93 \text{ MeV}^1$ . This relation should hold in the limit

$$f_\pi^2 M_\pi^2 V \gg 1, \quad (8)$$

---

<sup>1</sup> N.B. there is a common alternative convention, used for internal consistency in some more preliminary presentations of this data [2], where a factor of 2 is removed from  $f_\pi^2$  in Eqn. 7, and where  $f_\pi$  is a factor of  $\sqrt{2}$  larger, around 132 MeV.

which is the Leutwyler–Smilga parameter to leading order in  $M_\pi^2$ . We anticipate our results here to say that even on our most chiral lattices the LHS of Eqn. 8 is of order 10 and so this bound is well satisfied. Thus a calculation of  $\chi$  as a function of  $M_\pi$  should allow us to obtain a value of  $f_\pi$ . This method has an advantage over more conventional calculations in that it does not require us to know lattice operator renormalisation constants which are required for matching matrix elements, but which are usually difficult to calculate. In principle, we require instead knowledge of the renormalisation of the topological charge operators, but we see in the next Section that this problem can be readily overcome.

As  $m_q$  and  $M_\pi$  increase away from zero we expect higher order terms to check the rate of increase of the topological susceptibility so that, as  $m_q, M_\pi \rightarrow \infty$ ,  $\chi$  approaches the quenched value,  $\chi^{\text{qu}}$ . In fact, as we shall see below, the values of  $\chi$  that we obtain are not very much smaller than  $\chi^{\text{qu}}$ . So there is the danger of a substantial systematic error in simply applying Eqn. 7 at our smallest values of  $M_\pi$  in order to estimate  $f_\pi$ . To estimate this error it would be useful to have some understanding of how  $\chi$  behaves over the whole range of  $m_q$ . This is the question to which we now turn.

There are two quite different reasons why  $\chi$  might not be much smaller than  $\chi^{\text{qu}}$ . The obvious first possibility is that  $m_q$  is large. The second possibility is more subtle:  $m_q$  may be small but QCD may be close to its large- $N_c$  limit [8]. Because fermion effects are non-leading in powers of  $N_c$ , we expect  $\chi \rightarrow \chi^{\text{qu}}$  for any fixed, non-zero value of  $m_q$ , however small, as the number of colours  $N_c \rightarrow \infty$ . There are phenomenological reasons [8, 9] for believing that QCD is ‘close’ to  $N_c = \infty$ , and so this is not an unrealistic consideration. Moreover in the case of  $D = 2 + 1$  gauge theories it has been shown [10] that even  $\text{SU}(2)$  is close to  $\text{SU}(\infty)$ . Recent calculations in four dimensions [11, 12] indicate that the same is true there. In the present simulations, the lighter quark masses straddle the strange quark mass and so it is not obvious if we should regard them as being large or small. We shall therefore take seriously both the possibilities discussed above.

We start by assuming the quark mass is small but that we are close to the large- $N_c$  limit. In this limit, the topological susceptibility is known [7] to vary as

$$\chi = \frac{\chi^\infty M_\pi^2}{\frac{2N_f \chi^\infty}{f_\infty^2} + M_\pi^2} \quad (9)$$

where  $\chi^\infty$ ,  $f_\infty$  are the quantities at leading order in  $N_c$ . In the chiral limit, at fixed  $N_c$ , this reproduces Eqn. 7. In the large- $N_c$  limit, at fixed  $M_\pi$ , it tends to the quenched susceptibility  $\chi^\infty$  because  $f_\infty^2 \propto N_c$ . The corrections to Eqn. 9 are of higher order in  $M_\pi^2$  and/or lower order in  $N_c$ .

We now consider the alternative possibility: that  $m_q$  is not small, that higher-order corrections to  $\chi$  will be important for most of the values of  $m_q$  at which we perform calculations, and that we therefore need an expression for  $\chi$  that interpolates between  $m_q = 0$  and  $m_q = \infty$ . Clearly one cannot hope to derive such an expression from first principles, so we will simply choose one that we can plausibly argue is approximately

correct. The form we choose is

$$\chi = \frac{f_\pi^2}{\pi N_f} M_\pi^2 \arctan \left( \frac{\pi N_f}{f_\pi^2} \chi^{\text{qu}} \frac{1}{M_\pi^2} \right) \quad (10)$$

where  $f_\pi$  is the pion decay constant in the chiral limit. The coefficients have been chosen so that this reproduces Eqn. 7 when  $M_\pi \rightarrow 0$  and  $\chi \rightarrow \chi^{\text{qu}} + \mathcal{O}(1/M_\pi^4)$  when  $M_\pi \rightarrow \infty$ . Thus, this interpolation formula possesses the correct limits and it approaches those limits with power-like corrections.

We shall use the expressions in Eqns. 7, 9 and 10 to analyse the  $m_q$  dependence of our calculated values of  $\chi$  and to obtain a value of  $f_\pi$  together with an estimate of the systematic error on that value. In addition, the comparison with Eqn. 9 can provide us with some evidence for whether QCD is close to its large- $N_c$  limit or not.

### 3 Lattice measurements

We have calculated  $\chi$  on five complete ensembles of dynamical configurations produced by the UKQCD collaboration, as well as one which is still in progress [2]. Details of these data sets are given in Table 1. The SU(3) gauge fields are governed by the Wilson plaquette action, with ‘‘clover’’ improved Wilson fermions. The improvement is non-perturbative, with  $c_{\text{sw}}$  chosen to render the leading order discretisation errors quadratic (rather than linear) in the lattice spacing,  $a$ .

The theory has two coupling constants. In pure gluodynamics the gauge coupling,  $\beta$ , controls the lattice spacing, with larger values reducing  $a$  as we move towards the critical value at  $\beta = \infty$ . In simulations with dynamical fermions it has the same role for a fixed fermion coupling,  $\kappa$ . The latter controls the quark mass, with  $\kappa \rightarrow \kappa_c$  from below corresponding to the massless limit. In dynamical simulations, however, the fermion coupling also affects the lattice spacing, which will become larger as  $\kappa$  is reduced (and hence  $m_q$  increased) at fixed  $\beta$ .

The three least chiral UKQCD ensembles (by which we mean largest  $m_\pi/m_\rho$ ) are  $e_6$ ,  $e_5$  and  $e_4$ . By appropriately decreasing  $\beta$  as  $\kappa$  is increased, the couplings are ‘matched’ to maintain a constant lattice spacing [13, 14] (which is ‘equivalent’ to  $\beta \simeq 5.93$  in gluodynamics with a Wilson action [2]) whilst approaching the chiral limit. The physical volume and discretisation effects should thus be very similar on these lattices. The remaining ensembles have lower quark masses, but are at a slightly reduced lattice spacing. (To have maintained a matched lattice spacing here would have required reducing  $\beta$  to values where the non-perturbative value  $c_{\text{sw}}(\beta)$  is not known.) As the lattices are all  $L \gtrsim 1.5$  fm, we believe that the minor reduction in the lattice volume should not lead to significant finite volume corrections. We also remark that ensembles  $e_2$  and  $e_3$  have been matched to have approximately the same chirality, but at (mildly) different lattice spacings.

Four-dimensional lattice theories are scale free, and the dimensionless lattice quantities must be cast in physical units through the use of a known scale. For this work, we use the

Sommer scale [15] both to define the lattice spacing for the matching procedure, and to set the scale. The measured value of  $\hat{r}_0$  on each ensemble, as listed in Table 1, corresponds to the same physical value of  $r_0 = 0.49$  fm. ( $\hat{r}_0$  is the dimensionless lattice value of  $r_0$  in lattice units i.e.  $\hat{r}_0 = r_0(a)/a$ . We use the same notation for other quantities.) As we are in the scaling window of the theory, we can then use the naïve dimensions of the various operators to relate lattice and physical quantities, e.g.  $\hat{r}_0^4 \hat{\chi} = r_0^4 \chi + \mathcal{O}(a^2)$ , where we have incorporated the expected non-perturbative removal of the corrections linear in the lattice spacing.

Further details of the parameters and the scale determination are given in [2]. Measurements were made on ensembles of 400–800 configurations of size  $L^3T = 16^3 32$ , separated by ten hybrid Monte Carlo trajectories. Correlations in the data were managed through jack-knife binning of the data, using ten bins whose size is large enough that neighbouring bin averages may be regarded as uncorrelated.

We begin, however, with a discussion of lattice operators and results in the quenched theory.

### 3.1 Lattice operators and $\chi^{\text{qu}}$

The simplest lattice topological charge density operator is

$$\hat{q}(n) = \frac{1}{2} \varepsilon_{\mu\nu\sigma\tau} \text{Tr} U_{\mu\nu}(n) U_{\sigma\tau}(x) \quad (11)$$

where  $U_{\mu\nu}(n)$  denotes the product of SU(3) link variables around a given plaquette. We use a reflection-symmetrised version and form

$$\hat{Q} = \frac{1}{32\pi^2} \sum_n \hat{q}(n), \quad (12)$$

$$\hat{\chi} = \frac{\langle \hat{Q}^2 \rangle}{L^3 T} \quad (13)$$

with  $a^4(L^3T)$  the lattice volume. In general,  $\hat{Q}$  will not give an integer-valued topological charge due to finite lattice spacing effects. There are at least three sources of these. First is the breaking of scale invariance by the lattice which leads to the smallest instantons having a suppressed action (at least with the Wilson action) and a topological charge less than unity (at least with the operator in Eqn. 11). We do not address this problem in this study, although attempts can be made to correct for it [16], but simply accept this as part of the overall  $\mathcal{O}(a^2)$  error. In addition to this, the underlying topological signal on the lattice is distorted by the presence of large amounts of UV noise on the scale of the lattice spacing [17], and by a multiplicative renormalisation factor [18] that is unity in the continuum, but otherwise suppresses the observed charge. Various solutions to these problems exist [1]. In this study we opt for the ‘cooling’ approach. Cooling explicitly erases the ultraviolet fluctuations so that the perturbative lattice renormalisation factors

for the topological charge and susceptibility are driven to their trivial continuum values, leaving  $\mathcal{O}(a^2)$  corrections that may be absorbed into all the other lattice corrections of this order. We cool by moving through the lattice in a ‘staggered’ fashion, cooling each link by minimising the Wilson gauge action applied to each of the three Cabibbo–Marinari SU(2) subgroups in the link element in turn. (The Wilson gauge action is the most local, and thus particularly efficient at removing short distance fluctuations whilst preserving the long range correlations in the fields.) Carrying out this procedure once on every link constitutes a cooling sweep (or ‘cool’). The violation of the instanton scale invariance on the lattice, with a Wilson action, is such that an isolated instanton cooled in this way will slowly shrink, and will eventually disappear when its core size is of the order of a lattice spacing, leading to a corresponding jump in the topological charge. Such events can, of course, be detected by monitoring  $\hat{Q}$  as a function of the number of cooling sweeps,  $n_c$ . Instanton–anti-instanton pairs may also annihilate, but this has no net effect on  $\hat{Q}$ . However, these observations do motivate us to perform the minimum number of cools necessary to obtain an estimate of  $\hat{Q}$  that is stable with further increasing  $n_c$  (subject to the above).

To estimate this point we calculate the normalised correlation function between the topological charges measured after  $n_c$  cooling sweeps, and a nominally asymptotic 25 cooling sweeps:

$$R_Q(n_c) = \frac{\langle \hat{Q}(n_c)\hat{Q}(25) \rangle}{\frac{1}{2} (\langle \hat{Q}(n_c) \rangle^2 + \langle \hat{Q}(25) \rangle^2)}. \quad (14)$$

In Fig. 1 we show a typical plot for ensemble  $e_4$ . As discussed before, we have opted not to attempt to round the topological charge to integer values. We find  $\langle \hat{Q} \rangle(n_c)$  and  $\langle \hat{Q}^2 \rangle(n_c)$  to be stable within statistical errors for  $n_c \gtrsim 5$ , and the results presented here are for  $n_c = 10$ .

The topological charge of a configuration is related to the smallest eigenvalues of the Dirac matrix and as such is often believed to be one of the slowest modes to decorrelate during Monte Carlo simulations. It is crucial for the error analysis that the bin sizes for the data are at least twice the integrated autocorrelation times. In Fig. 2 we plot a typical time series of the topological charge measured every ten hybrid Monte Carlo trajectories. The rapid variation between configurations suggests that the integrated autocorrelation time is small even for the topological charge. Estimates of this are given in Table 2 in units of ten trajectories. These reinforce the impression gained from the time series plots. The bins used in the jack–knife statistical analysis are between 400 and 1000 trajectories in length and thus may be confidently assumed to be statistically independent. It is interesting that although autocorrelation times are hard to estimate accurately, it does appear that they increase as we move away from the chiral limit (c.f. Ref. [2]).

In Fig. 3 we divide the topological charge measurements made over an ensemble into bins of unit width centred on the integers, and plot a histogram of the probability of finding a configuration with each charge, with errors from the jack–knife analysis. We find for all our ensembles that these histograms are very close to being symmetric, centred

around  $\hat{Q} = 0$  and consistent with a Gaussian envelope. The hybrid Monte Carlo appears to be sampling the topological sectors correctly, and it is legitimate to extract an estimate of the topological susceptibility. On the histograms we show this estimate as a Gaussian curve

$$p(\hat{Q}) = \frac{1}{L^3 T \hat{\chi} \sqrt{2\pi}} \exp - \left[ \frac{\hat{Q}^2}{2L^3 T \hat{\chi}} \right] \quad (15)$$

The central line uses our estimate of  $\hat{\chi}$ , whilst the outlying curves use the central value plus or minus one standard deviation. The agreement with the histograms is good.

We also remark that on a lattice one obviously loses instantons with sizes  $\rho \leq \mathcal{O}(a)$ . Since the (pure gauge) instanton density decreases as  $\rho^6$  when  $\rho \rightarrow 0$  this would appear to induce a negligible  $\mathcal{O}(a^7)$  error in the susceptibility. However this is only true for  $a \rightarrow 0$ , and the error can be substantial for the coarse lattices often used in dynamical simulations.

In general, then, we expect the topological charge and susceptibility to be suppressed at non-zero lattice spacing. In gluodynamics with the Wilson action this suppression can, typically, be fitted by a leading order, and negative,  $\mathcal{O}(a^2)$  correction term starting from quite moderate values of  $\beta$ . Of course different ways of calculating the topological charge differ substantially at finite values of  $a$ , even if they agree in the continuum limit. (See, for example, Table 27 in [12].) An important factor for non-zero  $a$  is whether the topological charge is rounded to the nearest integer after cooling or not, as can be seen in Table 8 in [11]. A gluodynamic calculation of  $\hat{\chi}$  that uses a method very similar to the one used in the present paper, in particular an unrounded topological charge, can be found in the last column of Table 8 in [11]. The values of the susceptibility listed there can be fitted, for  $\beta \geq 5.7$ , by

$$\hat{r}_0^4 \hat{\chi}^{(\text{qu})} = 0.065 (3) - 0.28 (4) / \hat{r}_0^2. \quad (16)$$

In obtaining this fit we have used the interpolation formula for  $\hat{r}_0(\beta)$  that is given in [19]. We shall use this formula in Section 4 as a guide to the typical variation of  $\hat{\chi}$  with  $a$ .

In the next Section we shall want to compare our calculations of  $\hat{\chi}$ , as obtained in the presence of sea quarks, with an appropriate quenched limit. The ‘equivalent’ quenched limit will, of course, depend on the lattice spacing, i.e. on the value of  $\hat{r}_0$ . However, because of our strategy of varying  $\beta$  so as to approximately match the values of  $\hat{r}_0$  at the different values of  $m_q$ , the variation in this quenched value,  $\hat{r}_0^4 \hat{\chi}^{(\text{qu})}$ , over the range of lattice spacings of our ensembles, is in fact much less than the statistical errors on the measurements themselves. (If the calculations had been performed at fixed  $\beta$ , the lattice spacing would have become increasingly coarse with increasing  $m_q$ , and the reduction in the quenched susceptibility would have been much more pronounced over this range of  $\kappa$ . We shall return to this important point when we discuss other work in section 4.) One finds [2] that  $\hat{r}_0 = 4.714 (13)$  at  $\beta = 5.93$  in the quenched theory, demonstrating that this provides an appropriate quenched limit for our calculations (see Table 1). At  $\beta = 5.93$  the interpolation formula for  $\hat{r}_0(\beta)$  that we used to obtain Eqn. 16 gives  $\hat{r}_0 \simeq 4.735$



and if we insert this in Eqn. 16 we obtain  $\hat{r}_0^4 \hat{\chi}^{(\text{qu})} = 0.0525$  (11). Different methods for calculating  $\hat{r}_0$  differ by  $O(a^2)$  terms, and part of the difference between the UKQCD value,  $\hat{r}_0 = 4.714$  (13), and the Sommer value,  $\hat{r}_0 \simeq 4.735$ , might be due to this. If we rescale the susceptibility to account for this, then the value of  $\hat{r}_0^4 \hat{\chi}^{(\text{qu})}$  drops to  $\simeq 0.0516$ . To do better than this we need to take into account the fact that the calculations of the topological charge that enter into Eqn. 16 are obtained by methods that are not exactly the same as those used in the calculations of the present paper. The potentially significant differences are that 20 cooling sweeps and an unsymmetrised topological charge were used in [11], while we use 10 cooling sweeps and a symmetrised charge. To estimate the systematic shift induced by these differences we have performed calculations on 300  $16^4$  lattice field configurations generated at  $\beta = 5.93$  (separated by 50 Monte Carlo sweeps). We find that there is no significant difference between the susceptibility as calculated by the symmetrised and unsymmetrised charges, whether after 10 or 20 cooling sweeps. There is, on the other hand, a small but significant difference between the susceptibility as calculated after 10 and 20 cooling sweeps. This reduces our estimate of the equivalent quenched susceptibility by  $\sim 0.0025$  (7). So taking all this into account we take our equivalent quenched susceptibility to be given by

$$\hat{r}_0^4 \hat{\chi}^{(\text{qu})}(\beta = 5.93) = 0.049 \quad (2).$$

### 3.2 Sea quark effects in the topological susceptibility

In Table 2 we give our estimates of the topological susceptibility in physical units, using  $r_0$  as the scale. In Fig. 4 we plot  $\hat{r}_0^4 \hat{\chi}$  versus a similarly scaled pseudoscalar meson mass (calculated, of course, with valence quarks that are degenerate with those in the sea, i.e.  $\kappa_{\text{valence}} = \kappa_{\text{sea}}$ ). We also plot the corresponding value of the quenched topological susceptibility, as calculated at  $\beta = 5.93$ .

Comparing the dynamical and quenched values, the effects of the sea quarks are clear. Whilst the measurement on  $e_6$  and  $e_5$  are consistent with the quenched value, moving to smaller  $m_q$  ( $\propto M_\pi^2$ ) the topological susceptibility is increasingly suppressed.

We can make this observation more quantitative by attempting to fit our values of  $\hat{r}_0^4 \hat{\chi}$  with the expected functional form in Eqn. 7, so extracting a value of  $f_\pi$ . But we must first be clear whether this fit is justified, and what exactly we are extrapolating in, bearing in mind that Eqn. 7 is strictly a chiral expansion that describes the behaviour for small sea quark masses in the continuum limit.

An immediate concern is that our cooling technique will occasionally misidentify the value of  $Q$  and, in addition, that at finite lattice spacing the exact zero modes associated with the topological charge  $Q$  are shifted away from zero. All this implies that  $\hat{\chi}$  will not in fact vanish as  $m_q \rightarrow 0$ . However we expect this effect to be small for the following reasons. First, the use of an improved fermion action should ensure that the zero-mode shift will only be significant for very small instantons, i.e. those whose sizes are  $\rho \sim O(a)$ . These are unlikely to survive the cooling and should not contribute to our calculated value of  $Q$ .

Large instantons, on the other hand, for which any zero mode shift should be negligible, will certainly survive the cooling. The remaining ambiguity involves the smaller, but not very small, instantons. These might be erased by the cooling but the probability is small simply because the number of such charges is small [16, 20]. For example, we can see from Fig. 12 in [11] that the cooling only appears to cut out instantons with  $\rho \leq 2.5a$ . Since the lattice spacing in that plot is a factor of 1.5 smaller than at our equivalent quenched  $\beta$  value of 5.93, we would expect that cooling at  $\beta = 5.93$  would affect instantons that have  $\rho \leq 4a$  in that plot. We see from the SU(3) curve in that figure (after scaling up by a factor of  $\simeq 4$  to take us from a volume of  $20^4$  at  $\beta = 6.2$  to a volume of  $16^3 32$  at  $\beta = 5.93$ ) that this involves less than one topological charge per field configuration. This is a small effect in the present context. Thus it is reasonable to assume that this effect can be neglected for values of  $a$  and  $m_q$  comparable to the ones that we study, and that we can then apply Eqn. 7 to values of the susceptibility obtained by varying  $m_q$  at a fixed value of the lattice spacing: except that now the decay constant  $\hat{f}_\pi$  will be the one appropriate to that lattice spacing.

Now, whilst most of our data points are evaluated on a trajectory of constant lattice spacing in the parameter space [13], not all are. If  $\hat{r}_0 \hat{f}_\pi$  varied significantly with  $a$  over this range of  $a$ , it would not be clear how to perform a consistent chiral extrapolation through the data points. The non-perturbative improvement of the action, however, removes the leading order lattice spacing dependence and the residual corrections in this range of lattice spacings appear to be small, at least in measurements of (quenched) hadron spectroscopy [21, 22]. An indication of the possible size of the effect on topological observables comes from comparing our two measurements of  $\hat{r}_0^4 \hat{\chi}$  at  $(\hat{r}_0 \hat{M}_\pi)^2 \simeq 4$ . The range of lattice spacings here ( $\hat{r}_0$  varies from 4.75 to 5.14) is comparable to that over our total data set. The accompanying shift in the topological susceptibility is, however, within our statistical errors. Accordingly, we proceed now to attempt a common chiral extrapolation to the data, assuming throughout that lattice corrections to the relations discussed before are too small to be discernable in our limited data. We shall at the end of this Section return to the issue of scaling violations.

For this purpose, and in the light of the discussion at the end of section 3.1, it is useful to redisplay the data in Fig. 5, where the leading order chiral behaviour would then be a horizontal line,

$$\frac{\hat{r}_0^2 \hat{\chi}}{\hat{M}_\pi^2} = c_0 \quad (18)$$

and including the first correction gives a generic straight line

$$\frac{\hat{r}_0^2 \hat{\chi}}{\hat{M}_\pi^2} = c_0 + c_1 (\hat{r}_0 \hat{M}_\pi)^2. \quad (19)$$

In each case the intercept is related to the decay constant by  $c_0 = (\hat{r}_0 \hat{f}_\pi)^2/4$ . We now follow a standard fitting procedure, first using the most chiral points, then systematically adding the less chiral points until the fit becomes unacceptably bad. The larger the

number of points one can add in this way, the more evidence one has for the fitted form and the more confident one is that the systematic errors, associated with the neglected higher order corrections, are small. The results of performing such fits are shown in Table 3 and those using the two and four most chiral points respectively are plotted on Fig. 5. We see from the Table that the fits using Eqn. 19 show much greater stability and these are the ones that will provide our eventual best estimate for  $f_\pi$ .

We should comment briefly on the determination of the fitting parameter errors. In performing all but the constant fit we must contend with the data having (small) errors on the abscissa in addition to the ordinate. In order to estimate their affect on the fitting parameters, we first perform fits to the data assuming that the abscissa data take their central values. Identical fits are then made using the central values plus one, and then minus one standard deviation. The spread of the fit parameters obtained provides what is probably a crude over-estimate of this error (given there is some correlation between the ordinal and abscissal uncertainties) but is sufficient to show that it is minor. We show this spread as a second error, and for estimates of the decay constant we add it in quadrature to the other fit parameter error.

It is remarkable that we can obtain stable fits to most of our data using just the first correction term in Eqn. 19. Nonetheless, as we can see in Fig. 4, our values of the susceptibility are not very much smaller than the  $M_\pi = \infty$  quenched value and we need to have some estimate of the possible systematic errors that may arise from neglecting the higher order corrections that will eventually check the rise in  $\hat{\chi}$ . As discussed earlier we shall do so by exploring two possibilities. One is that the reason why  $\hat{\chi}$  is close to  $\hat{\chi}^{\text{qu}}$  is not that  $m_q$  is ‘large’ but rather that  $N_c = 3$  is large. Then the values of  $\hat{\chi}$  should follow the form in Eqn. 9. A second possibility is simply that our values of  $m_q$  are indeed large. In that case we have argued that the functional form Eqn. 10 should be a reasonable representation of the true mass dependence. We now perform both types of fit in turn.

We begin with the first possibility, and therefore fit the data with the following ansatz

$$\hat{r}_0^4 \hat{\chi} = \frac{c_0 c_3 (\hat{r}_0 \hat{M}_\pi)^2}{c_3 + c_0 (\hat{r}_0 \hat{M}_\pi)^2}, \quad (20)$$

where we expect  $c_3 = \hat{r}_0^4 \hat{\chi}^{\text{qu}}$  up to  $\mathcal{O}(1/N_c^2)$  corrections<sup>2</sup>. To test this we fit up to seven data points. The first six are measured in the dynamical simulations. The final quantity is the quenched susceptibility at  $\beta = 5.93$ .

We also expect, from the Maclaurin chiral expansion of Eqn. 20,

$$\hat{r}_0^4 \hat{\chi} = c_0 \cdot (\hat{r}_0 \hat{M}_\pi)^2 - c_0^2/c_3 \cdot (\hat{r}_0 \hat{M}_\pi)^4 + c_0^3/c_3^2 \cdot (\hat{r}_0 \hat{M}_\pi)^6 + \mathcal{O}((\hat{r}_0 \hat{M}_\pi)^8) \quad (21)$$

that  $c_0$  is related to the decay constant as before,  $c_0 = (\hat{r}_0 \hat{f}_\pi)^2/4$ . We present the results of the fits in Table 4. We find the UKQCD data to be well fitted by this form, but the asymptotic value is higher than the number we use for the quenched limit (in contrast to

---

<sup>2</sup>For an alternative motivation of this form, see [23].

earlier estimates of this value). Incorporating this number in the fit leads to a poorer  $\chi^2$ , and a less robust fit.

We turn now to fits based on the functional form in Eqn. 10. We therefore use the ansatz

$$\hat{r}_0^4 \hat{\chi} = \frac{2c_0}{\pi} (\hat{r}_0 \hat{M}_\pi)^2 \tan^{-1} \left( \frac{c_3}{\frac{2c_0}{\pi} (\hat{r}_0 \hat{M}_\pi)^2} \right) \quad (22)$$

where once again we expect  $c_3 = \hat{r}_0^4 \hat{\chi}^{\text{qu}}$  and from the expansion

$$\hat{r}_0^4 \hat{\chi} = c_0 (\hat{r}_0 \hat{M}_\pi)^2 - \left( \frac{2c_0}{\pi} \right)^2 \cdot \left( \frac{1}{c_3} \right) \cdot (\hat{r}_0 \hat{M}_\pi)^4 + \mathcal{O}((\hat{r}_0 \hat{M}_\pi)^8) \quad (23)$$

we expect  $c_0 = (\hat{r}_0 \hat{f}_\pi)^2/4$ . Note that in contrast to Eqn. 21, Eqn. 23 has no term that is cubic in  $m_q$  and the rise will remain approximately quadratic for a greater range in  $(\hat{r}_0 \hat{M}_\pi)^2$ . That this need be no bad thing is suggested by the relatively large range over which we could fit Eqn. 19. Indeed, we see from the fits listed in Table 4 that this form fits our data quite well.

Typical examples of the fits from Eqn. 20 and Eqn. 22 are shown in Figs. 4 and 5. The similarity of the two functions is apparent. In Table 5 we use the fit parameters to construct the first three expansion coefficients in the Maclaurin series for the various fit functions, describing the chiral behaviour of  $\chi$ . The fits are consistent with one another.

The fitted asymptote of the susceptibility at large  $m_q$  is given by  $c_3$ . We see from Table 4 that these are broadly consistent with the quenched value, and our large statistical errors do not currently allow us to resolve any  $\mathcal{O}(1/N_c^2)$  deviation from this.

As an aside, we ask what happens if we cast aside some of our theoretical expectations and ask how strong is the evidence from our data that (a) the dependence is on  $M_\pi^2$  rather than on some other power, and (b) the susceptibility really does go to zero as  $M_\pi \rightarrow 0$ ? To answer the first question we perform fits of the kind Eqn. 22 but replacing  $(\hat{r}_0 \hat{M}_\pi)^2$  by  $(\hat{r}_0 \hat{M}_\pi)^c$ . We find, using all seven values of  $\hat{\chi}$ , that  $c = 1.32$  (33) (10); a value broadly consistent with  $c = 2$ . The  $\chi^2/\text{d.o.f.}$  is poorer, however, than for the fit with a power fixed to 2 (possible as there is one fewer d.o.f.) suggesting that the data does not warrant the use of such an extra parameter. As for the second question, we add a constant  $\hat{c}$  to Eqn. 22 and find  $\hat{c} = -0.056$  (23) (25). Again this is consistent with our theoretical expectation; and again the  $\chi^2/\text{d.o.f.}$  is worse. In both cases, however, the fits are not robust, with the fit parameters ill-constrained by our data. (See Table 6 for details of the above two fits.)

Finally, we attempt to address the issue of discretisation effects. Our use of the non-perturbative  $c_{\text{sw}}$  should have eliminated the leading  $\mathcal{O}(a)$  errors. Although  $(a/r_0)^2$  is small there is, of course, no guarantee that the coefficient of this correction might not be enhanced. We may begin to attempt to address this more quantitatively through a combined fit that includes the first order discretisation correction in  $\hat{r}_0$ . Our motivation here is not so much to give a continuum limit (our data will not really support reliably

such a long extrapolation in  $a^2$ ) as to control the variations due to differing discretisation in our data over the relatively small range of lattice spacings in our study. For this reason we fit the simplest combined ansatz

$$\hat{r}_0^4 \hat{\chi} = c_0 (\hat{r}_0 \hat{M}_\pi)^2 + c_1 (\hat{r}_0 \hat{M}_\pi)^4 + \frac{c_2}{\hat{r}_0^2} \quad (24)$$

to the five most chiral of our data points. The resultant parameters are shown in Table 7. The change in discretisation errors across our data set is clearly small, as we expected from the success of the previous fits. This justifies the use of a single chiral extrapolation over this limited range in  $\hat{r}_0$ . Whilst it does not, however, rule out deviations between the results of this and its equivalent in the continuum limit, it does give some indication that these deviations will be small. Clearly far greater accuracy in the measurements is needed to allow a confident extrapolation to  $a = 0$ .

Given the consistency of our description of the small  $M_\pi$  regime from our measurements, it is reasonable to use the values of  $c_0$  to estimate the pion decay constant,  $f_\pi$ . This is done in units of  $r_0$  in Tables 3 and 4. We use the common chiral fit of Eqn. 19 over the largest acceptable range to provide us with our best estimate and its statistical error. We then use the fits with other functional forms to provide us with the systematic error. This produces an estimate

$$\hat{r}_0 \hat{f}_\pi = 0.262 \pm 0.015 \begin{matrix} +0.046 \\ -0.025 \end{matrix} \quad (25)$$

where the first error is statistical and the second is systematic. This is of course no more than our best estimate of the value of  $f_\pi$  corresponding to our lattice spacing of  $a \simeq 0.1$  fm. This value will contain corresponding lattice spacing corrections and these must be estimated before making a serious comparison with the experimental value. We merely note that using  $\hat{r}_0 = 0.49$  fm we obtain from Eqn. 25 the value

$$f_\pi = 105 \pm 6 \begin{matrix} +18 \\ -10 \end{matrix} \text{ MeV} \quad (26)$$

which is reasonably close to the experimental value  $\simeq 93$  MeV.

## 4 Comparison with other studies

During the course of this work, there have appeared a number of other studies of the topological susceptibility in lattice QCD; in particular by the Pisa group [24, 25], the CP-PACS collaboration [26, 27], the SESAM-T $\chi$ L collaboration [28] and the Boulder group [29].

The most recent studies [27, 29] are consistent with our findings, but the earlier ones found no significant decrease of the susceptibility with decreasing quark (or pion) mass when everything was expressed in physical, rather than lattice, units. Indeed when our detailed results and analysis were first publicised [3] all the other studies then available [24, 25, 26] (and indeed [28]) appeared to contradict our findings and it was therefore

necessary for us to provide some reason why this might be so. Although the situation is now different, the lessons are still useful and we will therefore briefly summarise the main point here. For more details we refer the reader to [3].

All these other calculations differ from our study in having been performed at fixed  $\beta$ . That implies that the lattice spacing  $a$  decreases as  $m_q$  is decreased. In typical current calculations this variation in  $a$  is substantial. (See for example Fig. 4 of [30].) At the smallest values of  $m_q$  the lattice spacing cannot be allowed to be too fine, because the total spatial volume must remain adequately large. This implies that at the larger values of  $m_q$  the lattice spacing is quite coarse. Over such a range of lattice spacings, the topological susceptibility in the pure gauge theory typically shows a large variation (as, for example, in eqn.16). Since for coarser  $a$  more instantons (those with  $\rho \leq \mathcal{O}(a)$ ) are excluded, and more of those remaining are narrow in lattice units (with a correspondingly suppressed lattice topological charge) we expect that this variation is quite general, and not a special feature of the pure gauge theory with a Wilson action. In lattice QCD, we therefore expect two simultaneous effects in  $\hat{\chi}$  as we decrease  $m_q$  at fixed  $\beta$ . First, because of the  $\mathcal{O}(a^2)$  lattice corrections just discussed,  $\hat{\chi}$  will (like  $\hat{\chi}^{\text{qu}}$ ) tend to increase. Second, it will tend to decrease because of the physical quark mass dependence. In the range of quark masses covered in current calculations this latter decrease is not very large (as we have seen in our work) and we suggest that the two effects may largely compensate each other so as to produce a susceptibility that shows very little variation with  $m_q$ , in contrast to the ratio  $\hat{\chi}/\hat{\chi}^{\text{qu}}$  which does.

To illustrate this consider the fixed- $\beta$  calculation in [30]. The range of quark masses covered in that work corresponds to  $(\hat{r}_0 \hat{M}_\pi)^2$  decreasing from about 6.5 to about 3.0. Simultaneously  $a/r_0$  decreases from about 0.437 to about 0.274. Over this range of  $1/\hat{r}_0 \equiv a/r_0$  the pure gauge susceptibility increases by almost a factor of two, as we see using Eqn. 16. Clearly this is large enough to compensate for the expected variation of the susceptibility.

As  $\beta$  is increased, the  $\mathcal{O}(a^2)$  variation with  $m_q$  of the corresponding quenched susceptibility  $\hat{r}_0^4 \hat{\chi}^{\text{qu}}$  will clearly diminish. Thus we suggested in [3] that if CP-PACS were to repeat their susceptibility calculations on their larger  $\beta$  ensembles, they would find an  $m_q$  variation of  $\hat{r}_0^4 \hat{\chi}$  consistent with ours. This is what they have done in their most recent work [27] with the result that we predicted. All this emphasises the utility of the UKQCD strategy of decoupling the variation of lattice corrections from the physical  $m_q$  dependence, by performing calculations at fixed  $a$  rather than at fixed  $\beta$ .

## 5 Summary

We have calculated the topological susceptibility in lattice QCD with two light quark flavours, using lattice field configurations in which the lattice spacing is approximately constant as the quark mass is varied. We find that there is clear evidence for the expected suppression of  $\chi$  with decreasing (sea) quark mass.

We have discussed this behaviour in the context of chiral and large  $N_c$  expansions, and find good agreement with the functional forms expected there. We are not able to make a stronger statement about how close QCD is to its large  $N_c$  limit, owing to the relatively large statistical errors on our calculated values, particularly at larger quark masses. This situation should change in the near future and, together with the increasing availability of information on the large- $N_c$  behaviour of the pure gauge (quenched) theory [11], a more precise comparison will become possible.

The consistent leading order chiral behaviour from our various fitting ansätze allows us to make an estimate for the pion decay constant,  $f_\pi = 105 \pm 6 \begin{smallmatrix} +18 \\ -10 \end{smallmatrix}$  MeV, for the lattice spacing of  $a \simeq 0.1$  fm. (Here the first error is statistical and the second has to do with the chiral extrapolation.) We use a lattice fermion action in which the leading  $\mathcal{O}(a)$  discretisation errors have been removed. Since the more accurate (quenched) hadron masses show little residual lattice spacing dependence [21, 22], we might expect that this value of  $f_\pi$  is close to its continuum limit. In any case, we note that it is in agreement with the experimental value,  $\simeq 93$  MeV.

## Acknowledgments

The work of A.H. was supported in part by UK PPARC grants PPA/G/0/1998/00621 and PPA/G/S/1999/00022. A.H. wishes to thank the Aspen Center for Physics for its hospitality during part of this work. We thank D. Hepburn and D. Pleiter for preliminary estimates of lattice pion masses.

## References

- [1] M. Teper, Nucl. Phys. (Proc. Suppl.) 83-84 (2000) 146 [hep-lat/9909124].
- [2] UKQCD Collaboration: C.R. Allton et al., hep-lat/0107021.
- [3] UKQCD Collaboration: A. Hart and M. Teper, hep-ph/0004180.
- [4] UKQCD Collaboration: A. Hart and M. Teper, hep-lat/0009008.
- [5] UKQCD Collaboration: A. Hart and M. Teper, Nucl. Phys. Proc. Suppl. 83-84 (2000) 476 [hep-lat/9909072].
- [6] P. Di Vecchia and G. Veneziano, Nucl. Phys. B 171 (1980) 253.
- [7] H. Leutwyler and A. Smilga, Phys. Rev. D 46 (1992) 5607.
- [8] G. 't Hooft, Nucl. Phys. B 75 (1974) 461.
- [9] E. Witten, Nucl. Phys. B 160 (1979) 57.

- [10] M. Teper, Phys. Rev. D 59 (1999) 014512 [hep-lat/9804008].
- [11] B. Lucini and M. Teper, JHEP 06 (2001) 050 [hep-lat/0103027].
- [12] M. Teper, hep-th/9812187.
- [13] UKQCD Collaboration: A.C. Irving et al., Phys. Rev. D 58 (1998) 114504 [hep-lat/9807015].
- [14] UKQCD Collaboration: J. Garden, Nucl. Phys. Proc. Suppl. 83-84 (2000) 165 [hep-lat/9909066].
- [15] R. Sommer, Nucl. Phys. B 411 (1994) 839 [hep-lat/9310022].
- [16] UKQCD Collaboration: D. Smith and M. Teper, Phys. Rev. D 58 (1998) 014505 [hep-lat/9801008].
- [17] P. Di Vecchia, K. Fabricius, G.C. Rossi, and G. Veneziano, Nucl. Phys. B 192 (1981) 392.
- [18] M. Campostrini, A. Di Giacomo, and H. Panagopoulos, Phys. Lett. B 212 (1988) 206.
- [19] S. Necco and R. Sommer, hep-lat/0108008.
- [20] A. Ringwald and F. Schrempp, Phys. Lett. B 459 (1999) 249 [hep-lat/9903039].
- [21] H. Wittig, Nucl. Phys. Proc. Suppl. 63 (1998) 47 [hep-lat/9710013].
- [22] R.G. Edwards, U.M. Heller, and T.R. Klassen, Phys. Rev. Lett. 80 (1998) 3448 [hep-lat/9711052].
- [23] S. Durr, hep-lat/0103011.
- [24] B. Alles, M. D’Elia, and A. Di Giacomo, Nucl. Phys. Proc. Suppl. 83-84 (2000) 431 [hep-lat/9912012].
- [25] B. Alles, M. D’Elia, and A. Di Giacomo, Phys. Lett. B 483 (2000) 139 [hep-lat/0004020].
- [26] CP-PACS Collaboration: A. Ali Khan et al., Nucl. Phys. Proc. Suppl. 83-84 (2000) 162 [hep-lat/9909045].
- [27] CP-PACS Collaboration: A. Ali Khan et al., hep-lat/0106010.
- [28] SESAM-T $\chi$ L Collaborations: G.S. Bali et al., hep-lat/0102002.
- [29] A. Hasenfratz, hep-lat/0104015.



- [30] UKQCD Collaboration: C.R. Allton et al., Phys. Rev. D 60 (1999) 034507 [hep-lat/9808016].
- [31] UKQCD Collaboration: K.C. Bowler et al., Phys. Rev. D 62 (2000) 054506 [hep-lat/9910022].
- [32] CP-PACS Collaboration: A. Ali Khan et al., hep-lat/0105015.

label	$\beta$	$\kappa$	$c_{\text{sw}}$	$N_{\text{traj.}}$	$\hat{r}_0$	$\hat{m}_\pi/\hat{m}_\rho$	$\hat{r}_0\hat{m}_\pi$
e <sub>1</sub>	5.20	0.13565	2.0171	2800	5.21 (5)	—	<i>1.386 (63)</i>
e <sub>2</sub>	5.20	0.13550	2.0171	8300	5.041 (40)	0.578 <sup>+13</sup> <sub>-19</sub>	1.480 (22)
e <sub>3</sub>	5.25	0.13520	1.9603	8200	5.137 (49)	—	<i>1.978 (22)</i>
e <sub>4</sub>	5.20	0.13500	2.0171	7800	4.754 (40)	0.700 <sup>+12</sup> <sub>-10</sub>	1.925 (38)
e <sub>5</sub>	5.26	0.13450	1.9497	4100	4.708 (52)	0.783 <sup>+5</sup> <sub>-5</sub>	2.406 (27)
e <sub>6</sub>	5.29	0.13400	1.9192	3900	4.754 (40)	0.835 <sup>+7</sup> <sub>-7</sub>	2.776 (32)

Table 1: *The ensembles studied, with measurements made every tenth HMC trajectory. Numbers in italics are preliminary estimates.*

ens.	$\tau_{\text{int}}(\hat{Q})$	$\langle Q^2 \rangle$	$\hat{r}_0^4 \hat{\chi}$
e <sub>1</sub>	32 (7)	4.50 (72)	0.0253 (41)
e <sub>2</sub>	48 (6)	6.30 (96)	0.0311 (48)
e <sub>3</sub>	—	7.04 (66)	0.0374 (37)
e <sub>4</sub>	79 (5)	11.48 (90)	0.0447 (37)
e <sub>5</sub>	89 (6)	11.74 (1.00)	0.0440 (42)
e <sub>6</sub>	129 (19)	17.13 (2.63)	0.0668 (104)
$\beta = 5.93$	—	6.47 (24)	0.049 (2)

Table 2: The topological charge integrated autocorrelation time estimates (in units of HMC trajectories), the square of the charge and the susceptibility. The quenched result at  $\beta = 5.93$  is for  $16^4$  [11], compared to  $16^3 32$  for the dynamical lattices.

Fit	$N_{\text{fit}}$	$c_0$	$c_1$	$\chi^2/\text{d.o.f.}$	$Q$	$\hat{r}_0 \hat{f}_\pi$
Eqn. 18	2	0.0141 (18)	—	0.300	0.584	0.238 (16)
Eqn. 18	3	0.0106 (8)	—	2.850	0.058	0.206 (8)
Eqn. 18	4	0.0111 (7)	—	2.311	0.074	0.211 (7)
Eqn. 18	5	0.0096 (5)	—	5.289	0.000	—
Eqn. 19	3	0.0187 (36) (5)	-0.0023 (11) (1)	0.416	0.519	0.274 (27)
Eqn. 19	4	0.0184 (37) (5)	-0.0020 (10) (1)	1.405	0.245	0.272 (28)
Eqn. 19	5	0.0172 (19) (1)	-0.0017 (4) (0)	0.984	0.399	0.262 (15)
Eqn. 19	6	0.0149 (16) (1)	-0.0011 (3) (0)	2.071	0.082	0.244 (14)

Table 3: Fits to the  $N_{\text{fit}}$  most chiral points of  $(\hat{r}_0^2 \hat{\chi})/\hat{M}_\pi^2$ .

Fit	$N_{\text{fit}}$	$c_0$	$c_3$	$\chi^2/\text{d.o.f.}$	$Q$	$\hat{r}_0 \hat{f}_\pi$
Eqn. 20	3	0.0262 (142) (34)	0.0592 (252) (35)	0.553	0.457	0.324 (91)
Eqn. 20	4	0.0216 (88) (29)	0.0812 (379) (176)	1.441	0.237	0.294 (64)
Eqn. 20	5	0.0257 (86) (24)	0.0664 (156) (24)	1.123	0.338	0.320 (56)
Eqn. 20	6	0.0220 (65) (20)	0.0773 (202) (37)	1.401	0.231	0.297 (46)
Eqn. 20	7	0.0445 (94) (21)	0.0501 (20) (0)	2.134	0.261	0.422 (46)
Eqn. 22	3	0.0210 (69) (21)	0.0456 (115) (16)	0.529	0.467	0.290 (51)
Eqn. 22	4	0.0190 (52) (20)	0.0564 (158) (37)	1.408	0.245	0.276 (41)
Eqn. 22	5	0.0205 (44) (16)	0.0517 (73) (12)	1.013	0.386	0.286 (34)
Eqn. 22	6	0.0184 (37) (15)	0.0575 (95) (19)	1.457	0.212	0.272 (30)
Eqn. 22	7	0.0219 (30) (12)	0.0497 (19) (1)	1.408	0.300	0.296 (22)

Table 4: Fits to the  $N_{\text{fit}}$  most chiral points of  $(\hat{r}_0^4 \hat{\chi})$ .

Fit	$N_{\text{fit}}$	const.	$\mathcal{O}((\hat{r}_0 \hat{M}_\pi)^2)$	$\mathcal{O}((\hat{r}_0 \hat{M}_\pi)^4)$
Eqn. 19	4	0.0172 (20)	-0.0017 (4)	—
Eqn. 20	5	0.0220 (68)	-0.0063 (43)	0.0018 (20)
Eqn. 20	6	0.0286 (39)	-0.0130 (35)	0.0059 (24)
Eqn. 22	5	0.0184 (40)	-0.0024 (12)	0
Eqn. 22	6	0.0170 (18)	-0.0019 (4)	0

Table 5: Chiral expansion terms of fitted functions.

$N_{\text{fit}}$	$c_0$	$c_3$	$c$	$\hat{c}$	$\chi^2/\text{d.o.f.}$	$Q$
7	0.086 (32) (45)	0.105 (23) (35)	fixed to 2	-0.056 (23) (35)	1.570	0.180
7	0.0160 (53) (26)	0.0492 (20) (0)	1.32 (33) (10)	fixed to 0	1.573	0.178

Table 6: Fits to the  $N_{\text{fit}}$  most chiral values of  $(\hat{r}_0^4 \hat{\chi})$ ; for the power  $c$  of  $M_\pi^2$ , and for the chiral intercept,  $\hat{c}$ . These are as described in the text.

$N_{\text{fit}}$	$c_0$	$c_1$	$c_2$	$\chi^2/\text{d.o.f.}$	$Q$
5	0.0148 (75)	-0.0014 (10)	0.0055 (120)	1.611	0.200

Table 7: Simultaneous chiral and lattice spacing correction fit to the  $N_{\text{fit}}$  most chiral values of  $(\hat{r}_0^4 \hat{\chi})$ , as described in the text.

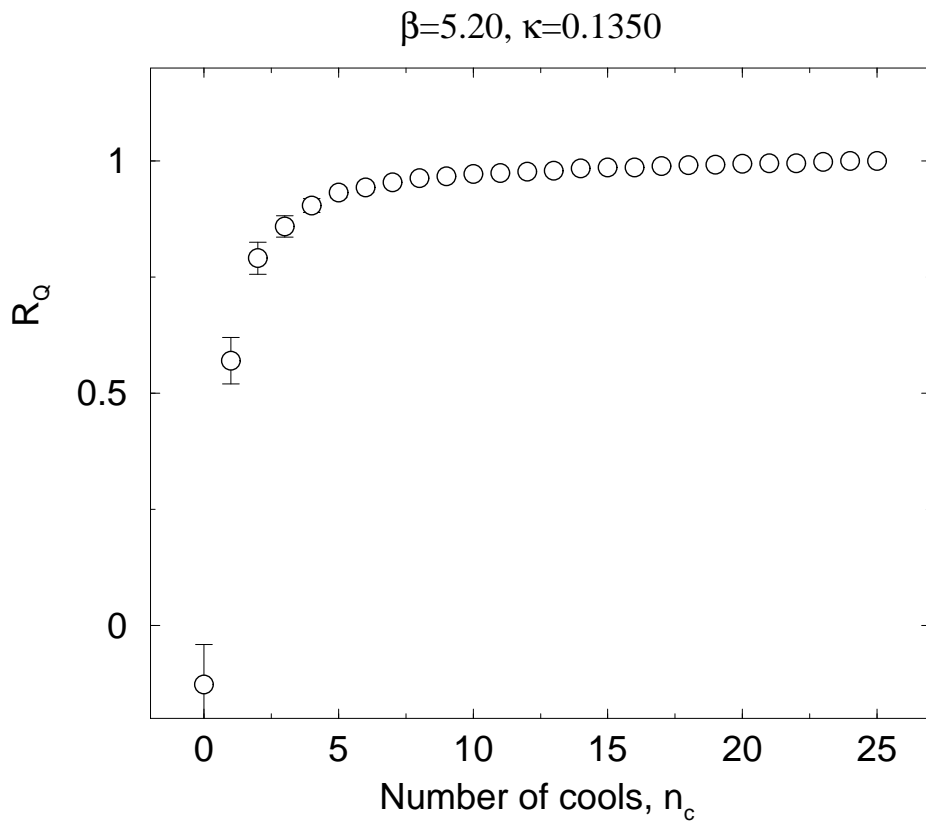


Figure 1: The normalised variation of the topological charge with cooling,  $R_Q(n_c)$  (Eqn. 14).

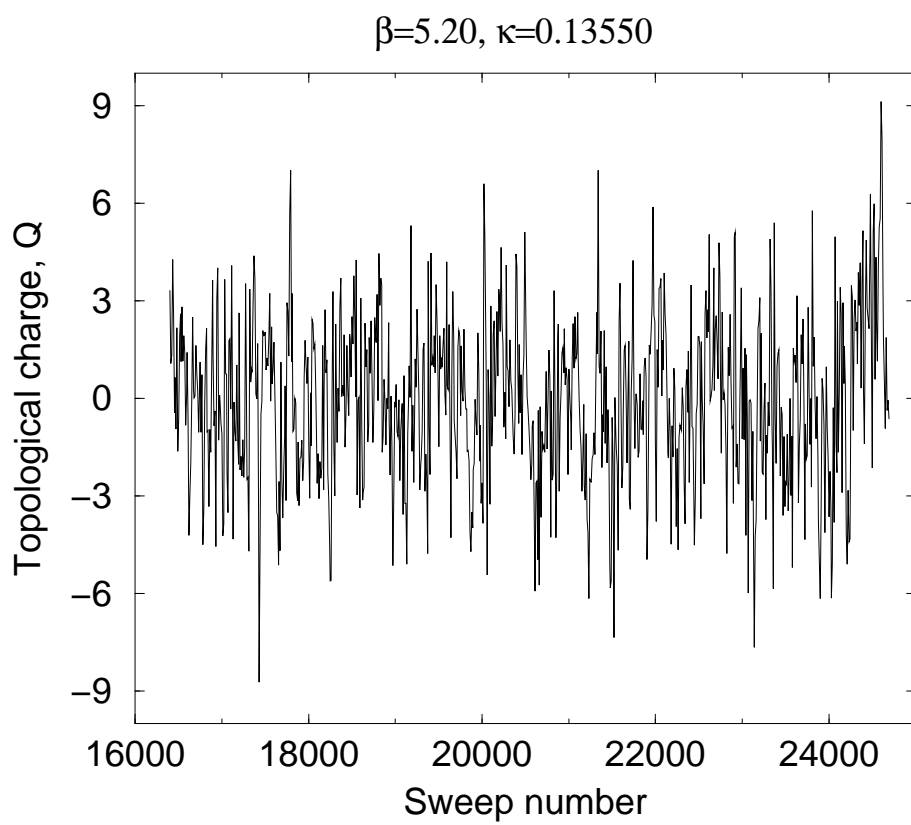


Figure 2: A Monte Carlo time series of  $\hat{Q}$  after ten cools.

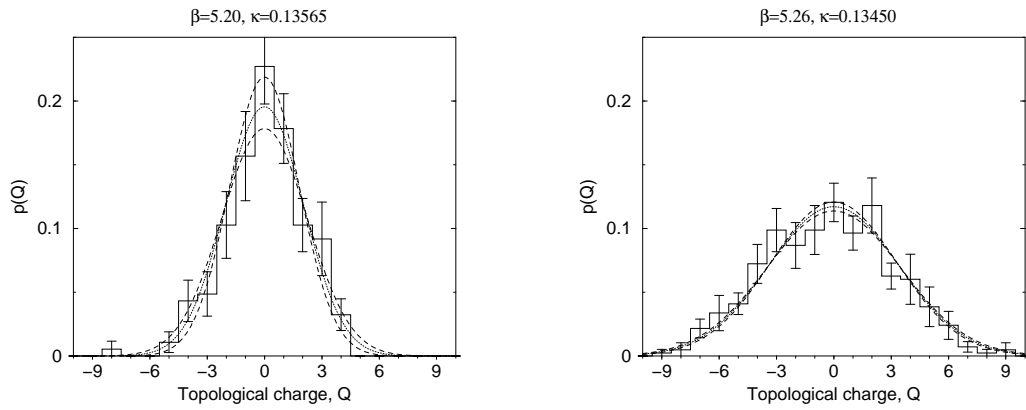


Figure 3: Histograms of the topological charge for the most and second least chiral ensembles, together with the Gaussian given in Eqn. 15.

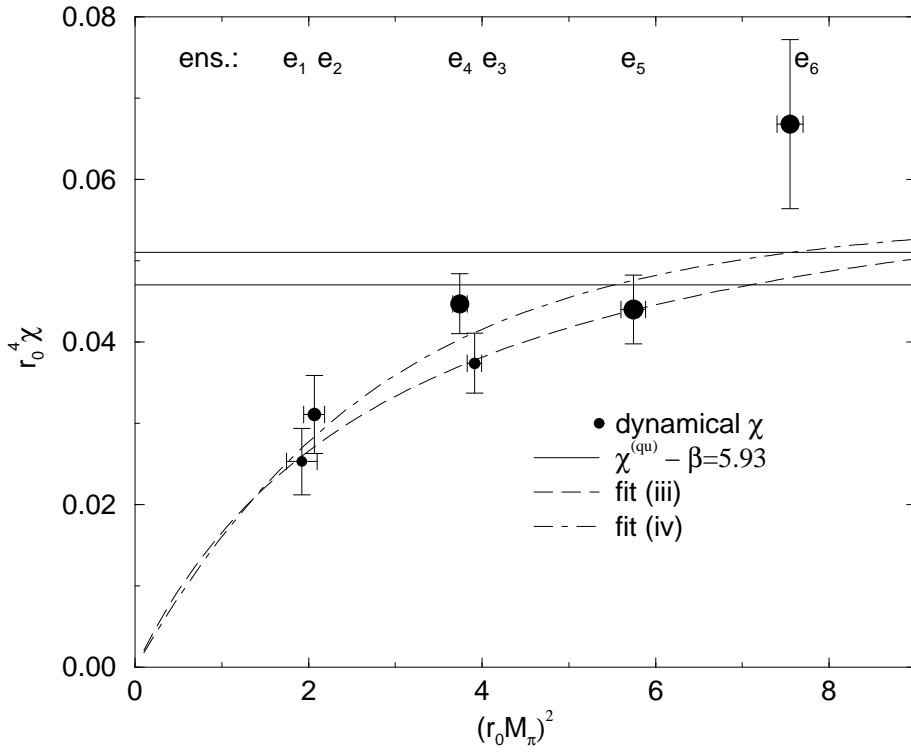


Figure 4: The measured topological susceptibility, with quenched value at equivalent  $\hat{r}_0$ . The radius of the dynamical plotting points is proportional to  $\hat{r}_0^{-1}$ . The fits, independent of the quenched points, are: (iii) Eqn. 20 and (iv) Eqn. 22.

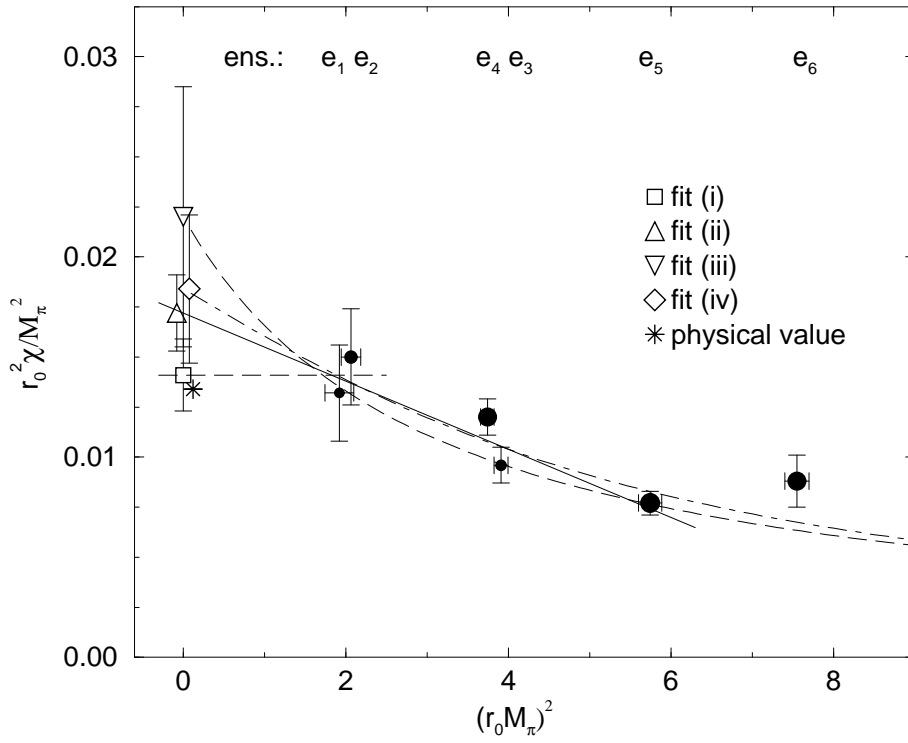


Figure 5: The measured topological susceptibility. The radius of the dynamical plotting points is proportional to  $\hat{r}_0^{-1}$ . The fits, independent of the quenched points, are: (i) Eqn. 18, (ii) Eqn. 19, (iii) Eqn. 20 and (iv) Eqn. 22.